Carbohydrate Polymers 92 (2013) 1953–1959

Contents lists available at SciVerse ScienceDirect

Carbohydrate Polymers

journal homepage: www.elsevier.com/locate/carbpol

Polyol mediated synthesis of ZnO nanoparticles templated by bacterial cellulose

Shiyan Chen*, Bihui Zhou, Weili Hu, Wen Zhang, Na Yin, Huaping Wang

State Key Laboratory for Modification of Chemical Fibers and Polymer Materials, Key Laboratory of Textile Science & Technology (Ministry of Education), College of Materials Science and Engineering, Donghua University, Shanghai 201620, PR China

ARTICLE INFO

Article history:
Received 13 June 2012
Received in revised form
13 November 2012
Accepted 21 November 2012
Available online 29 November 2012

Keywords:
Bacterial cellulose
ZnO nanoparticles
Template
Polyol meditated

ABSTRACT

Zinc oxide nanoparticles have been successfully synthesized through a facile polyol method using bacterial cellulose (BC) as a template. BC membrane was used as a host matrix to introduce quantitatively Zn^{2+} ions and then as nanoreactors to fabricate ZnO nanoparticles by hydrolysis of zinc acetate in a polyol medium. The influence of the concentration of zinc acetate and hydrolytic time on the morphologies and size of ZnO nanoparticles were investigated. The results indicated that the uniform spherical ZnO nanoparticles were incorporated into BC fibers. The resulting nanocomposites show good mechanical properties and high photocatalytic activity in the degradation of methyl orange.

1. Introduction

Zinc oxide (ZnO) nanomaterials, as a well-known n-type, II–IV semiconductor with a wide band gap of 3.37 eV and a high exciton binding energy of 60 meV, have aroused worldwide research interests in recent years due to their excellent optical, electrical, optoelectronic and photochemical properties (Kurbanov & Kang, 2009; Tao, Yu, Liu, Yang, & Yang, 2008; Wang, Li, Jia, Wang, & Tang, 2008). In particular, due to their high surface area and quantum confinement effect, ZnO nanomaterials have been the promising candidates for application in photo-catalysis, sensors, pigments, anti-bacterial materials and dye sensitized solar cells (Li, Hari, et al., 2007; Li, Wu, Hu, & Wang, 2007). In order to obtain ZnO nanomaterials with a specific morphology and size, much effort has been focused on the development of new synthetic strategies. Immobilization of ZnO nanomaterials through hybridization with an organic template, such as cellulosic fibers is an effective approach (Li, Hari, et al., 2007; Li, Wu, Hu, & Wang, 2007; Mao, Shi, Zhang, & Cao, 2009; Xu & Cai, 2008). For example, ZnO/cellulose nanocomposites could be prepared by hydrolysis of Zn(II)-amine complexes and the morphologies of ZnO structures depend on the type of amine (Gonçalves et al., 2009).

Bacterial cellulose (BC), produced through fermentation mostly by the *Acetobacter xylinum*, is extracellular cellulose composed of ribbon-like nanofibers approximately 10 nm thick and 50 nm wide structured in a fine network (Ifuku, Tsuji, Morimoto, Saimoto, & Yano, 2009; Oshima, Kondo, Ohto, Inoue, & Baba, 2008). It has various characteristics such as high crystallinity, high water holding capacity, high tensile strength (>2 GPa), high purity (free of lignin and hemicelluloses), and good biocompatibility. Benefit from these unique properties, BC can be used as "template" to synthesize nanomaterials through its three dimensional and porous structures and certain nano-pore size distribution (Hu, Chen, Li, et al., 2009; Hu, Chen, & Wang, 2009). Hussein, Yahaya, Ling, and Long (2005) prepared ZnO nanomaterials by hydrothermal synthesis using nata de coco as a shape-directing agent. However, this method requires rigorous reaction conditions and is restricted to academic studies.

Herein we reported a facile polyol method for fabricating ZnO nanoparticles using BC as the host matrix. Zn^{2+} ions incorporated into BC quantitatively, and then ZnO nanoparticles fabricated by hydrolysis of zinc acetate in a polyol medium (Bitenc & Orel, 2009; Feldmann & Metzmacher, 2001; Müller, Heim, Panneerselvam, & Willert-Porada, 2005; Poul, Ammar, Jouini, & Fievet, 2004). The influence of the concentration of zinc acetate and hydrolytic time on the morphologies and size of ZnO nanoparticles were investigated and the possible growth mechanism for the formation of ZnO nanoparticles coated on the BC fiber is proposed.

2. Experimental

2.1. Materials and instruments

All reagents were of analytical grade and were used as received. Zinc acetate dihydrate, diethylene glycol (DEG) and methyl orange

* Corresponding author. Tel.: +86 21 67792958; fax: +86 21 67792726.
E-mail addresses: chensy@dhu.edu.cn (S. Chen), wanghp@dhu.edu.cn (H. Wang).

0144-8617/$ – see front matter.
http://dx.doi.org/10.1016/j.carbpol.2012.11.059

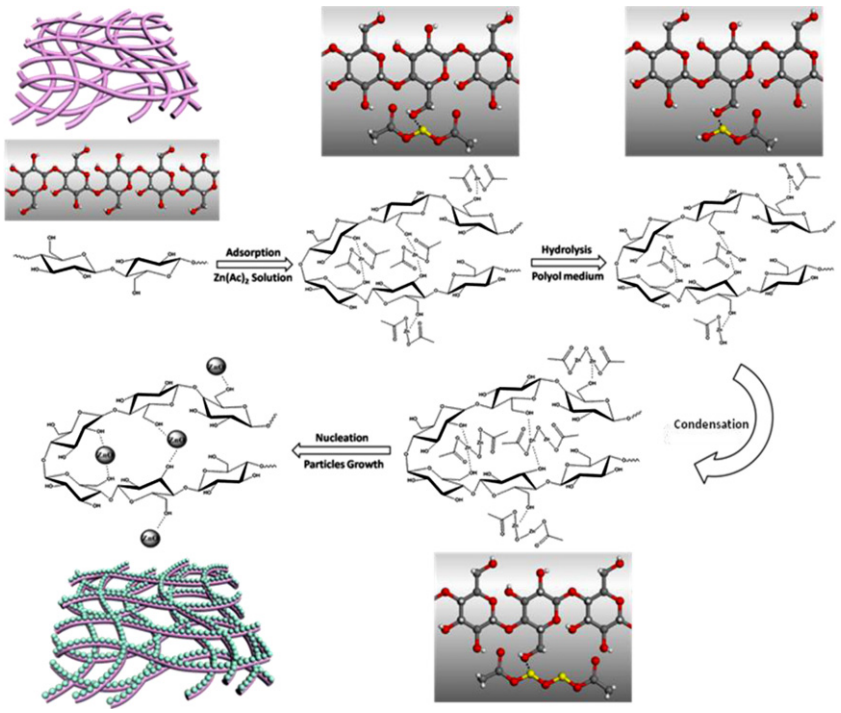

Fig. 1. Schematic illustration of the synthesis of the ZnO nanoparticles impregnated into BC.

were purchased from Sinopharm Chemical Reagent Co., Ltd. Purified BC membrane was kindly provided by Hainan Yeguo Foods Co. Ltd. Distilled water was used in all experiments.

The crystallinity and the phase composition of samples were characterized by XRD (D/Max-2550 PC, Rigaku, Japan) in the 2θ angle range from 4° to 60°. The Fourier transform infrared (FTIR) spectra were recorded on a Nicolet NEXUS-670 in the wave number range of 400 and 4000 cm^{-1} and the sample was grounded with dried potassium bromide (KBr) powder and compressed into a disc, and then was subjected to analysis. The morphology of the ZnO/BC membranes was investigated by means of FESEM (S-4800 field emission scanning electron microscope). Prior to analysis, samples cut from the freeze-dried ZnO/BC membranes were coated with gold palladium by cathodic spreading. TG was carried out with a Netzsch TG 209 F1 Iris under nitrogen atmosphere with a heating rate of 20 °C/min. The Brunauer–Emmett–Teller (BET) surface area, porosity, and pore size distribution of the samples were characterized by nitrogen gas adsorption (Micromeritics, ASAP 2020 analyzer) and the samples were thoroughly degassed at 150 °C for 12 h prior to measurements. Tensile strengths of the samples were measured using a WDW 3020 Universal Testing Machine at room temperature and a crosshead speed of 5 mm/min. Samples were cut into strip-shaped specimens 30 mm in length, 5 mm in width and 0.03 mm in thickness.

2.2. Preparation of ZnO/BC membranes

Freeze-dried BC membranes (3 cm × 4 cm) were dipped in 0.25, 0.5, 1 and 5 wt% zinc acetate aqueous solution at room temperature for 2 h to reach adsorption equilibrium. After being rinsed with distilled water for three times, the BC membranes, 5 mL zinc acetate aqueous solution (0.25, 0.5, 1 and 5 wt%), 50 mL diethylene glycol were mixed in a round bottom flask and stirred vigorously in an oil bath at 170–180 °C for a certain time. Subsequently, the membranes were taken out and stay stand for 30 min. The final composite membranes were washed with distilled water and ethanol three times to remove the solvent, any loosely bound ZnO and other impurities, and finally freeze dried overnight.

2.3. Photocatalytic activity measurement

The photocatalytic activities of the ZnO/BC nanocomposite films were evaluated by the photocatalytic degradation of methyl orange (MO) solution (Hu, Chen, Zhou, & Wang, 2010). A set of experiments was performed as follows: 2 g dried membrane in 100 mL MO (10 ppm) was magnetically stirred in the dark for 30 min to reach the adsorption equilibrium of MO with the catalyst. Then the system was irradiated using a UV lamp at a wavelength of 254 nm. At different irradiation time intervals, 10 mL samples of the irradiated water were withdrawn for analysis using a UV–vis spectrophotometer (UV-1200, Shanghai Mapada Instruments Co., Ltd.). The degradation efficiency (Dt) of MO solution was calculated as follows: $D\,(\%) = (A_0 - A_t)/A_0 \times 100$, where A_0 and A_t are the absorption value of 10 mg/L MO solution and samples at different irradiation time, respectively. The photocatalytic activities of different samples were evaluated by changes of Dt with the reaction time (t).

3. Results and discussion

3.1. Formation of ZnO nanoparticles on BC fibers

The schematic illustration of ZnO nanoparticles impregnating into BC is shown in Fig. 1. Firstly, when BC membrane is immersed in zinc acetate aqueous solution, the nanopores of BC can allow guest molecules Zn^{2+} to impregnate into the three-dimensional network structure until the adsorption equilibrium established. Thus zinc ions incorporate and anchor onto the stable absorption site through electrostatic interactions between Zn^{2+} and OH groups on BC fibers, as the oxygen atoms have a lone pair of electrons which can bind Zn^{2+} through an electron pair sharing (Chen, Shen, Yu, Hu, & Wang, 2010; Hu, Chen, Li, et al., 2009; Hu, Chen, & Wang, 2009; Ifuku et al., 2009). The free Zn^{2+} can be removed by rinsing in distilled water. Secondly, the Zn^{2+}/BC membrane was added into a polyol

and zinc acetate aqueous solution and heated to 170–180 °C. ZnO nanoparticles in situ formed by hydrolysis and condensation at the absorpted sites as below meditated by polyol (Lee et al., 2008):

$$Zn(CH_3COO)_2 + H_2O \rightarrow Zn(OH)(CH_3COO) + CH_3COOH \quad (1)$$

$$Zn(CH_3COO)_2 + Zn(OH)(CH_3COO) \rightarrow Zn_2(O)(CH_3COO)_2 + CH_3COOH \quad (2)$$

$$Zn(OH)(CH_3COO) + Zn(OH)(CH_3COO) \rightarrow Zn_2(O)(CH_3COO)_2 + H_2O \quad (3)$$

In the process, $Zn(CH_3COO)_2$ anchored on the surface of the BC nanofibres and the added $Zn(CH_3COO)_2$ in the reaction solution firstly was hydrolyzed to form $Zn(OH)(CH_3COO)$ as the intermediate (reaction (1)), then Zn—O—Zn bond is yielded through the condensation of the $Zn(OH)(CH_3COO)$ species (reactions (2) and (3)), subsequently the nucleation center (ZnO) formed and the growth of the ZnO nanoparticles at the absorbed sites. In this process, the limited available $Zn(OH)(CH_3COO)$ intermediate hydrolyzed by the $Zn(CH_3COO)_2$ anchored on the surface of BC nanofibres. They may establish a competition relationship with the added $Zn(CH_3COO)_2$ in the reaction solution. At the same time, the rapid hydrolysis and condensation reactions at the absorbed sites may lead to the formation of numerous nuclei and finally would prevent preferential growth along the c-axis (Lee et al., 2008; Poul et al., 2004). Thus ZnO nanoparticles have the tendency to grow into relatively equiaxial particles and to be anchored at the absorbed sites, preventing the nanoparticles from aggregating.

3.2. XRD analysis

Fig. 2 is the X-ray diffraction patterns of the nanocomposites samples synthesized at different Zn^{2+} concentration and hydrolytic time. The broad diffraction peaks at 14.60°, 16.82° and 22.78° are assigned to the BC fibers (Tokoh, Takabe, Fujita, & Saiki, 1998). The other peaks at 31.72°, 34.38°, 36.20°, 47.54° and 56.54° are corresponded to the (1 0 0), (0 0 2), (1 0 1), (1 0 2) and (1 1 0) crystal planes of wurtzite structure ZnO (JCPDS, 36-1451), respectively. No peaks from any other impurities such as $Zn(OH)_2$ are observed which demonstrates the high purity and crystallinity of the obtained nanocomposites. As shown in Fig. 2, the crystallinity of ZnO is greatly affected by the concentration of zinc acetate and hydrolytic time. From Fig. 2(1), we can see that the crystallinity degree improves with the increase of Zn^{2+} concentration which is reflected by the markedly increased intensity of the diffraction peaks. Furthermore, a short time (5 min) is not enough for the process of ZnO crystallization, thus some broadening peaks assigned to amorphous solid are observed (Fig. 2(2)).

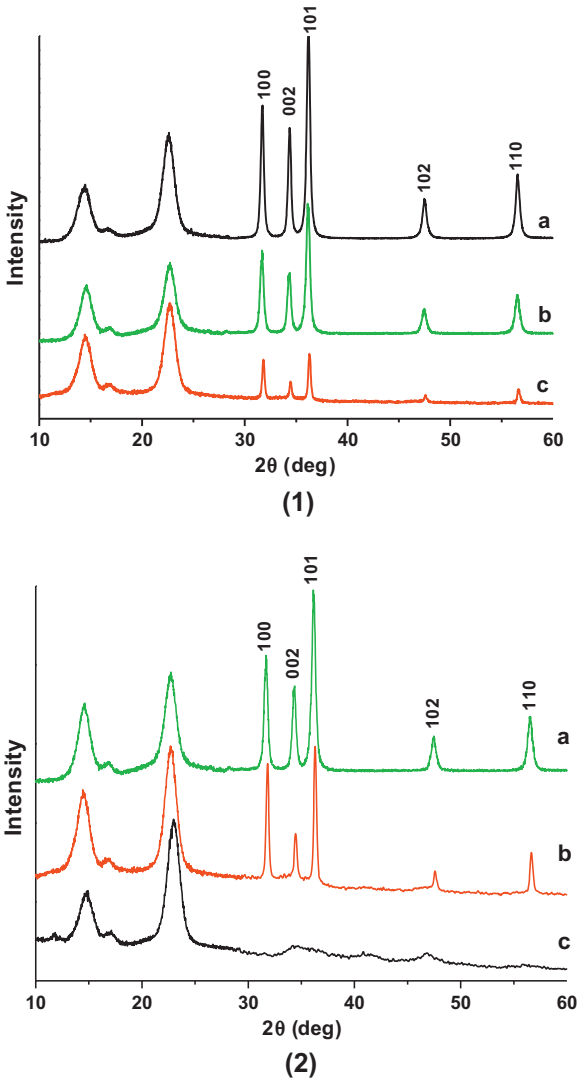

Fig. 2. X-ray diffraction pattern of ZnO/BC synthesized at (1) different Zn^{2+} concentration (hydrolytic time: 20 min) (a) 1 wt%, (b) 0.5 wt%, and (c) 0.25 wt%; (2) different hydrolytic time (Zn^{2+} concentration: 0.5 wt%) (a) 20 min, (b) 10 min, and (c) 5 min.

3.3. FT-IR characterization

In order to reveal the reactive site during hydrolytic process and evaluate the interaction between Zn^{2+}, ZnO nanoparticles and BC matrix, FTIR measurements were performed as shown in Fig. 3. It can be seen that after dipping BC into zinc acetate solution, the peaks at 3410 cm^{-1} corresponding to stretching vibrations of hydroxyl groups of BC are weakened to lower wavenumbers (3348 cm^{-1}), and 3360 cm^{-1} in the resultant ZnO/BC composites, which indicates that the hydroxyl groups of BC have some interactions with both Zn^{2+} and ZnO nanoparticles. A similar phenomenon was observed for the in-plane OH deformation vibration (from 1648 cm^{-1} to 1576 cm^{-1} and 1570 cm^{-1}, respectively) (Hu et al., 2010).

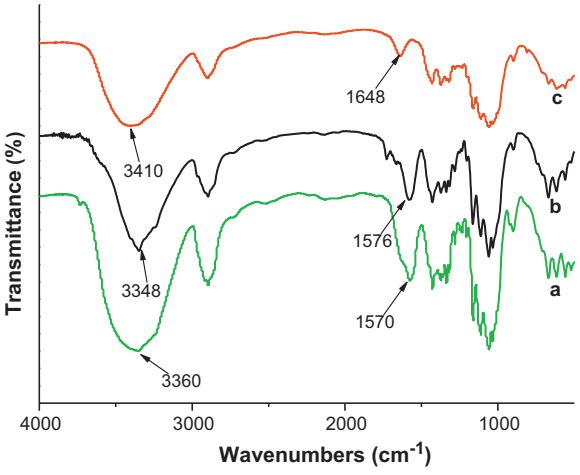

Fig. 3. FT-IR spectra of (a) ZnO/BC, (b) Zn^{2+}/BC, and (c) BC.

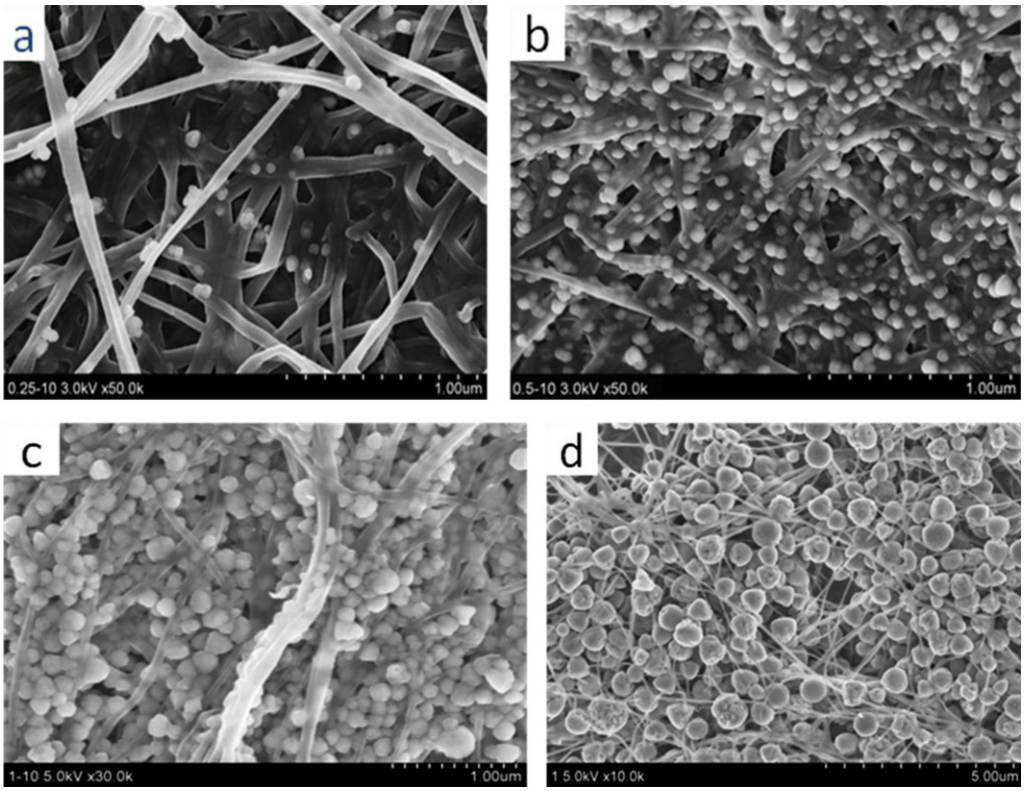

Fig. 4. FESEM images of ZnO nanoparticles synthesized at different concentrations of zinc acetate: (a) 0.25 wt%, (b) 0.5 wt%, (c) 1 wt%, and (d) 5 wt%.

3.4. Morphology analysis

The size and morphology of ZnO particles are greatly affected by the external conditions during the forming process. Here, we investigated the effect of concentration of zinc acetate and hydrolytic time on the morphologies of ZnO nanoparticles.

In this polyol mediated synthesis of ZnO nanoparticles templated by BC, the concentration of zinc ions plays an important role in determining the particles size and distribution. Fig. 4 shows the

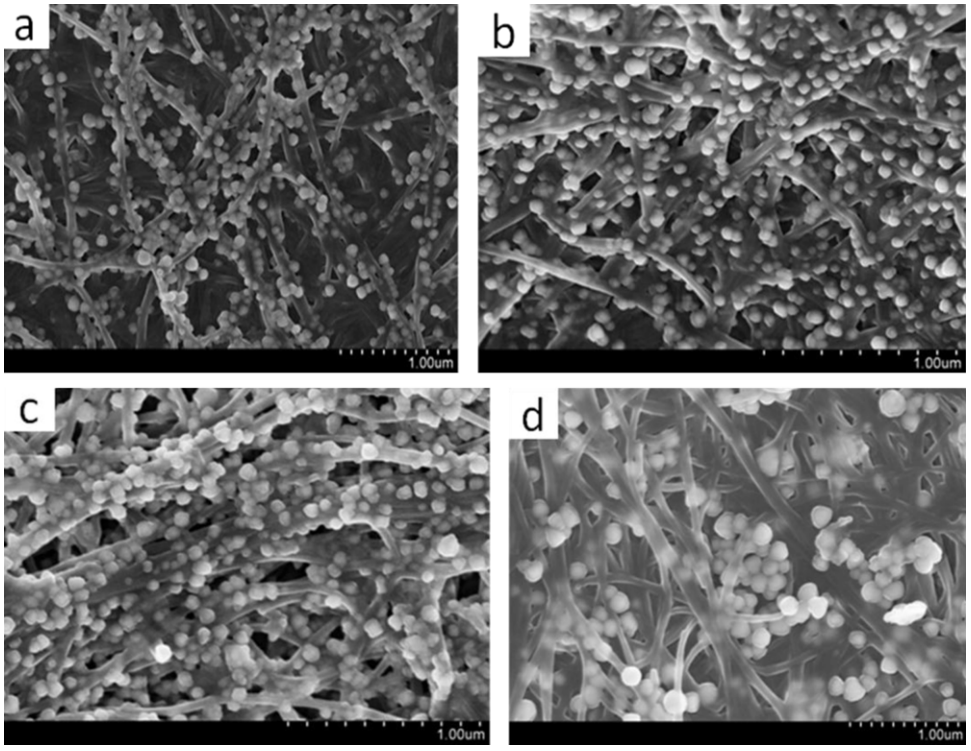

Fig. 5. FESEM images of ZnO nanoparticles synthesized at different hydrolytic time: (a) 5 min, (b) 10 min, (c) 15 min, and (d) 30 min.

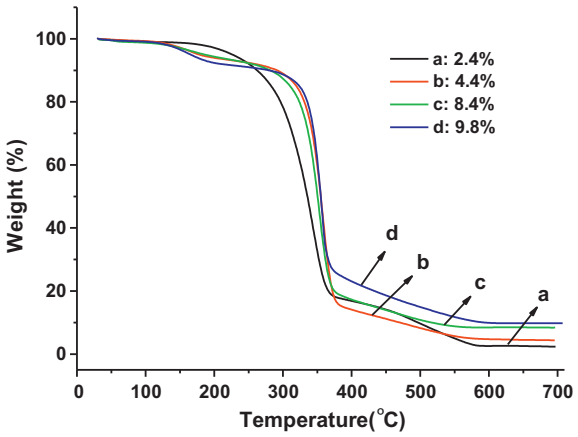

Fig. 6. TG curves of (a) BC, BC/ZnO composites synthesized with the concentration of Zn^{2+}, (b) 0.25 wt%, (c) 0.5 wt%, and (d) 1 wt%.

FESEM images of the ZnO nanoparticles synthesized under different concentrations of zinc acetate varies from 0.25 wt% to 5 wt% (the hydrolytic time was fixed as 10 min). It is observed that the average diameters of the samples are approximately 50–100 nm corresponding to the Zn^{2+} concentration of 0.25 and 0.5 wt% in the reaction solution. When the Zn^{2+} concentration increase to 1 wt%, the average diameters of the ZnO nanoparticles also grow to about 100–200 nm and further to more than 500 nm when the Zn^{2+} concentration increase to 5 wt%. The result can be explained that the more Zn^{2+} active site formed along BC fibers with the increase of the concentration of Zn^{2+}, subsequently larger amount of ZnO nuclei and growth sites can be obtained to form more ZnO nanoparticles. However, when the concentration of Zn^{2+} is too high, the small crystals or unstable particles on fibers may aggregate to larger crystals or particles (Tzeng, Hon, & Leu, 2009). When the concentration of Zn^{2+} is 0.5 wt%, the obtained ZnO nanoparticles are anchored discretely onto the BC control sites and have a uniform distribution and smaller particle size.

In order to investigate the effect of hydrolytic time on the particle size and distribution, we chose the optimal concentration of 0.5 wt% of zinc acetate and change the hydrolytic time from 5 min to 60 min. The FESEM images are shown in Fig. 5. When the hydrolytic time was 5 and 10 min, respectively, the ZnO nanoparticles with the diameter about 100 nm are relatively well-dispersed and grow regularly along the fibers. When the hydrolytic time was prolonged to 15 min (100 nm), more nuclei sites grown nearby tend to aggregate but not have enough time to grow into bigger particles. So more nanoparticles formed under the condition and only few slightly larger nanoparticles (>100 nm) are observed. The ZnO nanoparticles further begin to aggregate and form clusters (the diameter about 150–200 nm) with longer hydrolytic time (30 min) due to an increased possibility of inter-particle collisions.

3.5. Thermal properties

Fig. 6 shows the TG curves measured from room temperature to 700 °C of pure BC and ZnO/BC composites synthesized with different concentrations of Zn^{2+}. The curve of BC shows three obvious weight loss platforms. The first weight loss is about 5% from room temperature to 220 °C due to BC dehydration. Physically absorbed and hydrogen bonded linked water molecules can be lost at this stage. The second stage corresponding to a broad peak (250–350 °C) can be attributed to the pyrolysis of BC. The weight loss occurred at 350–600 °C was assigned to the third stage owing to the decarboxylation and decarbonylation reactions forming carbon monoxide and carbon dioxide (Barud et al., 2007; Hu, Chen, Xu, & Wang, 2011).

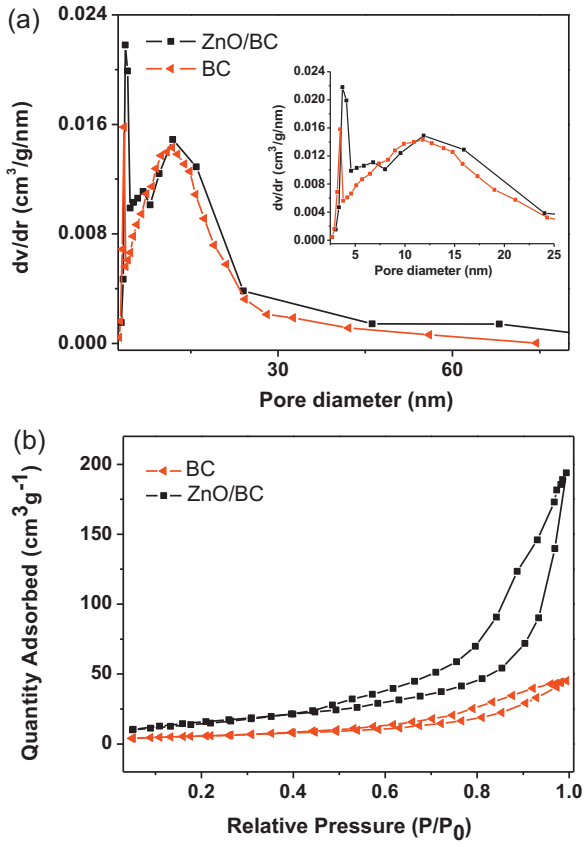

Fig. 7. (a) The BJH pore size distribution and (b) nitrogen adsorption–desorption isotherms of freeze-dried BC and ZnO/BC composite.

The TG curve of ZnO/BC nanocomposite is almost similar to pure BC membrane. But the introduction of ZnO nanoparticles into BC slightly improved the thermal stability of BC which indicated there is an interaction between BC and ZnO nanoparticles. And compared with BC membrane, the residue of composite at 700 °C could be referred to the content of ZnO nanoparticles which are about 2%, 6% and 7.4%, respectively.

3.6. Brunauer–Emmett–Teller (BET) and porosity characterization

The pore size calculation of the freeze-dried BC and ZnO/BC nanocomposite (0.5 wt% Zn^{2+}, 10 min) were performed on desorption branch of nitrogen adsorption–desorption by Barrett–Joiner–Halenda (BJH) method. The *dv*/*dr* vs. pore diameter curve and the N_2 adsorption–desorption isotherm are shown in Fig. 7. According to Fig. 7(a), a broad distribution of mesopores starting from around 4 nm extending to around 70 nm is found for pure BC fibers, whereas ZnO/BC nanocomposite shows the bimodal distribution with peaks at around 6.6 nm and 11.9 nm. The sharp peak around 3.8 nm arises from the tensile strength effect (TSE) and it is not the indication of mesoporosity (Groen, Peffer, & Pérez-Ramírez, 2003). After loading with ZnO nanoparticles, another peak could be observed at around 6.6 nm resulted from the increase of the hysteresis loop with the deposition of ZnO nanoparticles, which indicate an increase in the surface area and the total pore volume (Zhang & Qi, 2005). The BET surface areas of pure BC fibers and the ZnO/BC composites are found to be 55.36 and 101.34 m^2/g, respectively.

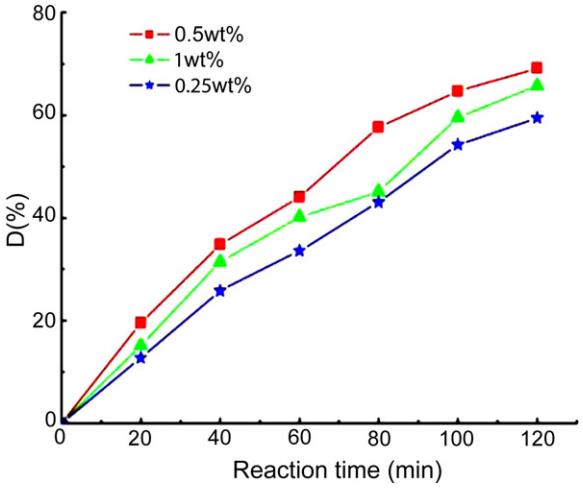

Fig. 8. Photocatalytic activity of ZnO/BC with the concentration of Zn^{2+}.

3.7. Mechanical properties

Fig. S1 presents the mechanical properties of the freeze-dried BC and ZnO/BC composites. The tensile strength and the Young's modulus of BC are 260 MPa and 8.7 GPa, respectively, which decrease to 153 MPa and 4.3 GPa due to loading ZnO nanoparticles. The loaded ZnO nanoparticles in the composite could enhance the molecular motion of cellulose in blend and perturb the strong hydrogen bond of cellulose (Kanjanamosit, Muangnapoh, & Phisalaphong, 2010). Moreover, the internal cracks of the aggregate particles make themselves stress concentrators (Ruan, Zhang, Zhang, & Xia, 2004). These factors result in a reduction of the mechanical properties of the composites.

Supplementary data associated with this article can be found, in the online version, at http://dx.doi.org/10.1016/j.carbpol.2012.11.059.

3.8. Photocatalytic properties

The photocatalytic activities of the ZnO/BC nanocomposite films were evaluated by the photocatalytic degradation of MO solution. The results of the photocatalytic degradation efficiencies are shown in Fig. 8. It can be found that the ZnO/BC nanocomposites synthesized at 0.5 wt% Zn^{2+} concentration displays a higher photocatalytic activity with a maximum decolorization efficiency of 70% at 120 min, followed by 1 wt% and 0.25 wt%. The reason may be attributed to the different specific surface areas, crystallite size and the composited amount of ZnO nanoparticles. The lowest photocatalytic properties by 0.25 wt% Zn^{2+} may come from the lower amount of ZnO (about 2 wt% according to the TG curves shown in Fig. 6). However, higher Zn^{2+} concentration leads to an increase in the particle size as confirmed by SEM, subsequently a drop in surface area, and further results in the decrease of the photocatalyst efficiency of 1 wt% compared with that of 0.5 wt% Zn^{2+}, although the amount of ZnO of 1 wt% Zn^{2+} is larger than that of 0.5 wt % Zn^{2+} (about 6 wt% ZnO of 0.5 wt% Zn^{2+}, about 7.4 wt% ZnO of 1 wt% Zn^{2+} according to Fig. 6).

4. Conclusion

In conclusion, we have successfully fabricated crystalline ZnO nanoparticles by a simple polyol method using BC as a bio-template. The size and morphology of ZnO nanoparticles are greatly affected by the hydrolytic time and concentration of zinc acetate. The ZnO/BC nanocomposites with a surface area of 101.34 m^2/g were obtained under the optimal condition (hydrolysis time: 10 min, concentration of Zn^{2+}: 0.5 wt%). The Brunauer–Emmett–Teller surface areas of pure BC fibers and the ZnO/BC composites are found to be 55.36 and 101.34 m^2/g, respectively, indicating an excellent candidate for photocatalyst. A relatively high photocatalytic activity with a maximum decolorization efficiency of 70% at 0.5 wt% Zn^{2+} was obtained.

Acknowledgements

This work was financially supported by The National Natural Science Foundation of China (51273043), Program of Introducing Talents of Discipline to Universities (B07024), Shanghai Leading Academic Discipline Project (B603), and Project of the Action on Scientists and Engineers to Serve Enterprises (2009GJE20016).

References

Barud, H. S., Ribeiro, C. A., Crespi, M. S., Martines, M. A. U., Dexpert-Ghys, J., Marques, R. F. C., et al. (2007). Thermal characterization of bacterial cellulose–phosphate composite membranes. *Journal of Thermal Analysis and Calorimetry*, *87*(3), 815–818.

Bitenc, M., & Orel, Z. C. (2009). Synthesis and characterization of crystalline hexagonal bipods of zinc oxide. *Materials Research Bulletin*, *44*(2), 381–387.

Chen, S., Shen, W., Yu, F., Hu, W., & Wang, H. (2010). Preparation of amidoximated bacterial cellulose and its adsorption mechanism for $Cu^{2+}$and Pb^{2+}. *Journal of Applied Polymer Science*, *117*(1), 8–15.

Feldmann, C., & Metzmacher, C. (2001). Polyol mediated synthesis of nanoscale MS particles (M = Zn, Cd, Hg). *Journal of Materials Chemistry*, *11*(10), 2603–2606.

Gonçalves, G., Marques, P. A. A. P., Neto, C. P., Trindade, T., Peres, M., & Monteiro, T. (2009). Growth, structural, and optical characterization of ZnO-coated cellulosic fibers. *Crystal Growth & Design*, *9*(1), 386–390.

Groen, J. C., Peffer, L. A. A., & Pérez-Ramírez, J. (2003). Pore size determination in modified micro- and mesoporous materials. Pitfalls and limitations in gas adsorption data analysis. *Microporous and Mesoporous Materials*, *60*(1–3), 1–17.

Hu, W., Chen, S., Li, X., Shi, S., Shen, W., Zhang, X., et al. (2009). In situ synthesis of silver chloride nanoparticles into bacterial cellulose membranes. *Materials Science and Engineering C*, *29*(4), 1216–1219.

Hu, W., Chen, S., & Wang, H. (2009). Template synthesis based on bacterial cellulose. *Journal of Clinical Rehabilitative Tissue Engineering Research*, *13*(8), 1597–1600.

Hu, W., Chen, S., Xu, Q., & Wang, H. (2011). Solvent-free acetylation of bacterial cellulose under moderate conditions. *Carbohydrate Polymers*, *83*(4), 1575–1581.

Hu, W., Chen, S., Zhou, B., & Wang, H. (2010). Facile synthesis of ZnO nanoparticles based on bacterial cellulose. *Materials Science and Engineering B*, *170*(1–3), 88–92.

Hussein, M. Z. B., Yahaya, A. H., Ling, P. L. C., & Long, C. W. (2005). *Acetobacter xylenum* as a shape-directing agent for the formation of nano-, micro-sized zinc oxide. *Journal of Materials Science*, *40*(23), 6325–6328.

Ifuku, S., Tsuji, M., Morimoto, M., Saimoto, H., & Yano, H. (2009). Synthesis of silver nanoparticles templated by TEMPO-mediated oxidized bacterial cellulose nanofibers. *Biomacromolecules*, *10*(9), 2714–2717.

Kanjanamosit, N., Muangnapoh, C., & Phisalaphong, M. (2010). Biosynthesis and characterization of bacteria cellulose–alginate film. *Journal of Applied Polymer Science*, *115*(3), 1581–1588.

Kurbanov, S. S., & Kang, T. W. (2009). Photoluminescence properties of bare and ZnO infilled artificial opal. *Optics Communications*, *282*(10), 2040–2044.

Lee, S., Jeong, S., Kim, D., Hwang, S., Jeon, M., & Moon, J. (2008). ZnO nanoparticles with controlled shapes and sizes prepared using a simple polyol synthesis. *Superlattices and Microstructures*, *43*(4), 330–339.

Li, M., Hari, B., Lv, X., Ma, X., Sun, F., Tang, L., et al. (2007). Direct synthesis of monodispersed ZnO nanoparticles in an aqueous solution. *Materials Letters*, *61*(3), 690–693.

Li, Y., Wu, D., Hu, J., & Wang, S. (2007). Novel infrared radiation properties of cotton fabric coated with nano Zn/ZnO particles. *Colloids and Surfaces A: Physicochemical and Engineering Aspects*, *300*(1–2), 140–144.

Mao, Z., Shi, Q., Zhang, L., & Cao, H. (2009). The formation and UV-blocking property of needle-shaped ZnO nanorod on cotton fabric. *Thin Solid Films*, *517*(8), 2681–2686.

Müller, A., Heim, O., Panneerselvam, M., & Willert-Porada, M. (2005). Polyol method for the preparation of nanosized Gd_2O_3, boehmite and other oxides. *Materials Research Bulletin*, *40*(12), 2153–2169.

Oshima, T., Kondo, K., Ohto, K., Inoue, K., & Baba, Y. (2008). Preparation of phosphorylated bacterial cellulose as an adsorbent for metal ions. *Reactive and Functional Polymers*, *68*(1), 376–383.

Poul, L., Ammar, S., Jouini, N., & Fievet, F. (2004). Synthesis of inorganic compound (metal oxide and hydroxide) in polyol medium: a versatile route related to the sol–gel process. *Journal of Sol–Gel Science and Technology*, *26*(1–3), 261–265.

Ruan, D., Zhang, L., Zhang, Z., & Xia, X. (2004). Structure and properties of regenerate cellulose tourmaline nanocrystal composite films. *Journal of Polymer Science: Part B Polymer Physics*, *42*(3), 367–373.

Tao, Z., Yu, X., Liu, J., Yang, L., & Yang, S. (2008). A facile synthesis and photoluminescence of porous S-doped ZnO architectures. *Journal of Alloys and Compounds*, *459*(1–2), 395–398.

Tokoh, C., Takabe, K., Fujita, M., & Saiki, H. (1998). Cellulose synthesized by *Acetobacter xylinum* in the presence of acetyl glucomannan. *Cellulose*, *5*(4), 249–261.

Tzeng, S. K., Hon, M. H., & Leu, I. C. (2009). Growth characteristics of ultra long double-ended acicular ZnO synthesized by a hydrothermal process. *Journal of Crystal Growth*, *311*(20), 4510–4517.

Wang, H., Li, G., Jia, L., Wang, G., & Tang, C. (2008). Controllable preferential-etching synthesis and photocatalytic activity of porous ZnO nanotubes. *Journal of Physical Chemistry C*, *112*(31), 11738–11743.

Xu, B., & Cai, Z. (2008). Fabrication of a superhydrophobic ZnO nanorod array film on cotton fabrics via a wet chemical route and hydrophobic modification. *Applied Surface Science*, *254*(18), 5899–5904.

Zhang, D., & Qi, L. (2005). Synthesis of mesoporous titania networks consisting of anatase nanowires by templating of bacterial cellulose membranes. *Chemical Communications*, (21), 2735–2737.